

Online ISSN: 2383-0042

Iranian Journal of Materials Forming

Journal Homepage: http://ijmf.shirazu.ac.ir



Research Article

Influence of Homogenization Duration on Interdendritic Phase Elimination and Hardness Behavior in AD730 Nickel-based Superalloy

Saeed Mortezaei, Seyyed Mehdi Abbasi* and Maryam Morakabati

Faculty of Materials and Manufacturing Technologies, Malek Ashtar University of Technology, Tehran, Iran

ARTICLE INFO

Article history:

Received: 4 September 2025 Reviewed: 25 October 2025 Revised: 1 November 2025 Accepted: 4 November 2025

Keywords:

AD730 superalloy Homogenization treatment Microstructural refinement Interdendritic phase elimination Hardness reduction

Please cite this article as:

Mortezaei, S., Abbasi, S, M., & Morakabati, M. (2026). Influence of homogenization duration on interdendritic phase elimination and hardness behavior in AD730 nickel-based superalloy. *Iranian Journal of Materials Forming*, 13(1), 4-14. https://doi.org/10.22099/IJMF.2 025.54121.1346

ABSTRACT

In this study, the effect of homogenization time on the microstructural evolution and mechanical properties of the cast AD730 superalloy at 1100 °C was investigated. The as-cast microstructure consisted of a dendritic structure along with interdendritic phases, including η phase, Laves phase, γ/γ' eutectic, and MC carbides. Microscopic examinations and localized analyses revealed that the eutectic and Laves phases were completely dissolved during the early stages of homogenization, while the η phase disappeared after 10 hours of treatment. Prolonging the homogenization time promoted chemical uniformity and gradual elimination of the dendritic structure, resulting in a nearly uniform microstructure after 25 hours. However, at this stage, the formation of voids was detected, indicating adverse effects due to over-homogenization. Hardness measurements showed a continuous decrease in hardness with increasing homogenization time, attributed to the gradual dissolution of the strengthening γ' precipitates. Based on these results, an optimal homogenization duration of 15 to 20 hours at 1100 °C is suggested, which can eliminate undesirable phases and enhance compositional uniformity while avoiding structural defects.

© Shiraz University, Shiraz, Iran, 2026

1. Introduction

Nickel-based superalloys are pivotal in advanced engineering sectors such as aerospace and power generation due to their superior high-temperature mechanical properties, including elevated strength, creep resistance, and thermal stability [1–3]. Among these alloys, AD730TM has emerged as a novel cast-and-

wrought superalloy tailored for applications up to 750 °C [4]. It combines high strength, excellent fatigue and long-term creep resistance, and cost-effective manufacturability, making it a promising material for critical components such as gas turbine disks.

The exceptional mechanical behavior of AD730TM is largely attributed to finely dispersed and stable γ'



^{*} Corresponding author E-mail address: sma_abbasi@mut.ac.ir (S. M. Abbasi) https://doi.org/10.22099/IJMF.2025.54121.1346

precipitates within the austenitic (γ) matrix. This microstructural feature not only enhanced high-temperature strength but also improves resistance to plastic deformation and thermal stability. The alloy's chemical composition is optimized to include approximately 30 wt.% of solid-solution strengthening elements such as cobalt (Co), chromium (Cr), tungsten (W), and molybdenum (Mo) alongside about 7 wt.% γ' -forming elements, including aluminum (Al), titanium (Ti), and niobium (Nb). This compositional balance facilitates the formation of a stable microstructure with desirable mechanical properties under service conditions [5, 6].

However, due to the alloy's complex chemistry and rapid solidification rates, elemental segregation during solidification is inevitable. Elements such as Nb, Ti, Mo, and Al tend to segregate to interdendritic regions, leading to the formation of brittle secondary phases that compromise the strength and structural integrity of components. Consequently, homogenization heat treatment is essential to mitigate segregation and achieve a uniform microstructural [4, 7, 8].

Previous studies have demonstrated that homogenization temperature and duration critically influence the dissolution of dendritic structures and the control of undesirable phases. Xia et al. [3] reported that extending homogenization time from 5 to 36 hours in GH4151 gradually eliminated dendritic structures, although excessive durations induced grain coarsening with irregular boundaries. Li et al. [9] found that homogenizing GH4975 at 1220 °C for 10 hours resulted in complete γ' dissolution and significant reduction in segregation. Fu et al. [10] emphasized that complete dendrite dissolution in Rene 65 alloy requires up to 50 hours at 1160-1190 °C, whereas shorter times are inadequate. They also noted that prolonged homogenization can promote grain growth and void formation due to rapid dissolution of interdendritic phases. Similarly, Miao et al. [11] demonstrated that a two-step homogenization process effectively removes unwanted phases and eutectic structures in IN718 alloy. Regarding AD730™, Blaizot et al. [12] highlighted that γ' precipitation not only governs mechanical properties at service temperatures but also critically influences recrystallization kinetics during forging. They stressed that precise control of homogenization parameters near the γ' solvus temperature is vital for achieving an optimal microstructure and mechanical performance.

Despite these advancements, systematic investigations on the effect of homogenization time on the microstructural evolution and interdendritic phases behavior in AD730TM remain limited. Therefore, this study aims to elucidate the influence of homogenization duration at 1100 °C close to the γ' solvus on the microstructural transformations of this alloy. Samples produced via vacuum induction melting (VIM) and vacuum arc remelting (VAR) were subjected to homogenization treatments for 5, 10, 15, 20, and 25 hours. Microstructural characterization was performed using optical and electron microscopy to assess dendritic morphology, γ/γ' distribution, and the dissolution behavior of secondary phases.

2. Experimental Procedure

The AD730 superalloy used in this study was produced by vacuum induction melting (VIM) followed by vacuum arc remelting (VAR) with a casting diameter of 100 mm. The chemical composition of the cast ingot was determined by quantitative spectrometry and is presented in Table 1 in weight percent. To investigate the effect of homogenization time on microstructural evolution, test specimens measuring 12 × 12 × 10 mm were sectioned transversely from the mid-radius (R/2) region of the cast ingot using wire electrical discharge machining (wire EDM). The specimens were subjected to homogenization treatment at a constant temperature of 1100 °C for durations ranging from 5 to 25 hours. The homogenization temperature of 1100 °C was specifically selected because it is close to the γ' solvus, enabling a investigation of the microstructural detailed transformations associated with γ' dissolution during prolonged thermal exposure. Prior to the treatment, the specimens were placed inside the furnace after it reached the target temperature, and immediately quenched in water upon completion of the specified holding time. A portable thermocouple was employed to ensure accurate

Table 1. Chemical composition of AD730 superalloy (wt.%)

AD730	Ni	Fe	Co	Cr	Mo	W	Al	Ti	Nb	В	С	Zr
Casting	Base	4.20	9.87	15.53	2.85	2.67	2.41	3.56	0.98	0.005	0.02	0.035

temperature control at the beginning of each experiment. Sample preparation, including grinding and polishing of the homogenized specimens, was carried out in accordance with standard metallographic procedures. Subsequently, the specimens were chemically etched by immersion in a solution composed of two-thirds hydrochloric acid (HCl) and one-third nitric acid (HNO₃) for 25 to 35 seconds to reveal microstructural features. Quantitative evaluation of microsegregation was carried out using energy-dispersive X-ray spectroscopy (EDS) integrated with a field emission scanning electron microscopy (FE-SEM) operated at an accelerating voltage of 15 kV.

To investigate the thermal behavior and phase transformations in the cast AD730 superalloy, simultaneous thermal analysis (STA) was performed on a representative sample from the as-cast ingot. The measurements were conducted at a heating and cooling rate of 5°C/min to accurately identify endothermic and exothermic events associated with y' precipice dissolution. Moreover, the effect of homogenization time on mechanical properties was evaluated through Brinell hardness testing using a Gnehm Brinell hardness tester (model BRCKER 220) with a dwell time of 8 seconds. To ensure accuracy, three measurements were taken at different locations on the cross-section of each specimen, and the average value was reported as the final hardness. Prior to testing, all specimens were fully ground and polished to prepare the surface and eliminate surface effects on the results.

3. Results and Discussion

3.1. As-cast microstructure

The microstructure of the as-cast nickel-based superalloy AD730 sample is shown in Fig. 1. The optical micrograph presented in Fig. 1(a) reveals a fully dendritic structure indicative of non-equilibrium solidification conditions. In this image, the bright regions correspond to primary dendrite cores, while the dark regions represent interdendritic areas. These microstructural

heterogeneities arise from alloying element segregation during non-equilibrium solidification, a common phenomenon in nickel-based superalloys due to variations in element partitioning rates at the solid-liquid interface [10, 13].

Fig. 1(b) presents a higher magnification view of the interdendritic region, where localized enrichment of alloying elements has promoted the formation of secondary phases. These secondary phases typically have a detrimental effect on mechanical properties, especially at elevated temperatures; therefore, their identification and control are crucial for process optimization. To determine the chemical composition of these phases, energy dispersive X-ray spectroscopy (EDS) analysis was conducted on four marked regions labeled A, B, C, and D.

Phase A exhibits a plate-like morphology and is enriched in titanium (Ti) and aluminum (Al). This chemical composition and structural morphology suggest the presence of a eutectic $\gamma + \gamma'$ structure, commonly observed in nickel-based superalloys containing a high-volume fraction of the γ' phase [10, 14]. This phase usually forms in the final stages of solidification due to localized enrichment of γ' -forming elements. The corresponding EDS analysis, shown in Fig. 1(c), confirms enrichment in Ti and Al, are principal constituents of the γ' phase.

In contrast, Phase B has a blade-shaped or needle-like morphology and is rich in niobium (Nb) and titanium (Ti). The EDS analysis presented in Fig. 1(d) indicates this phase as the η (eta) phase. This intermetallic compound typically forms due to segregation of alloying elements in interdendritic regions in advanced nickel-based superalloys. Due to its brittle nature and tendency to precipitate along grain boundaries or interdendritic areas, it can reduce ductility [2].

Phase C is characterized by a high concentration of Nb and Ti (Fig. 1(e)) and minimal content of other alloying elements. Therefore, this phase was identified as a carbide phase [15, 16]. Based on its chemical composition, the carbides are of the MC type, where the metallic component (M) primarily consists of Nb and Ti. These carbides predominantly form during solidification and are distributed as discrete particles within both intraand intergranular regions, particularly interdendritic boundaries. The formation of similar carbides during solidification has also been reported in other superalloys [2, 9, 16, 17]. Regarding phase D, a microstructural image along with elemental distribution maps and alloying element concentrations are presented in Fig. 2. The white regions visible in the microstructural, indicated by yellow arrows, represent the presence of this phase in the AD730 alloy. Chemical composition analysis using EDS revealed that the concentrations of Mo, Cr, and Nb in this phase are approximately 20.46%, 26.03%, and 12.34% by weight (%), respectively. These values are significantly higher than those in the initial chemical composition of the as-cast ingot. The elemental distribution maps clearly confirm this segregation, showing enriched areas of these elements prominently in the interdendritic regions.

According to previous studies [1, 2, 16], Mo, Cr, and Nb are as the key constituents in the formation of the Laves phase in nickel-based superalloys. This phase typically forms locally in interdendritic regions due to severe segregation of alloying elements during solidification.

Based on previous studies [4, 5, 19, 20], the Laves phase exhibits a stoichiometric composition of AB₂ and can crystallize into three main crystal structures: MgCu₂ (cubic), MgZn₂ (hexagonal), and MgNi₂ (hexagonal). In this context, element A corresponds to atoms with larger atomic radii, whereas element B consists of atoms with smaller atomic radii. In nickel-based superalloys, the Laves phase commonly forms as a result of the segregation of elements such as Mo, Nb, and W during the final stages of solidification or during specific heat treatment processes [8].

The chemical composition analysis of the Laves phase in the AD730 superalloy reveals that Mo, Nb, Ti, and W serve as group A elements, while Ni, Cr, Co, and Fe form the group B elements. Accordingly, the chemical formula of this phase in AD730 can be expressed as (Mo, Nb, Ti, W)(Ni, Cr, Co, Fe)₂, with an atomic ratio of approximately 1.98 between the A and B groups. These results confirm that this phase corresponds to the Laves phase in AD730.

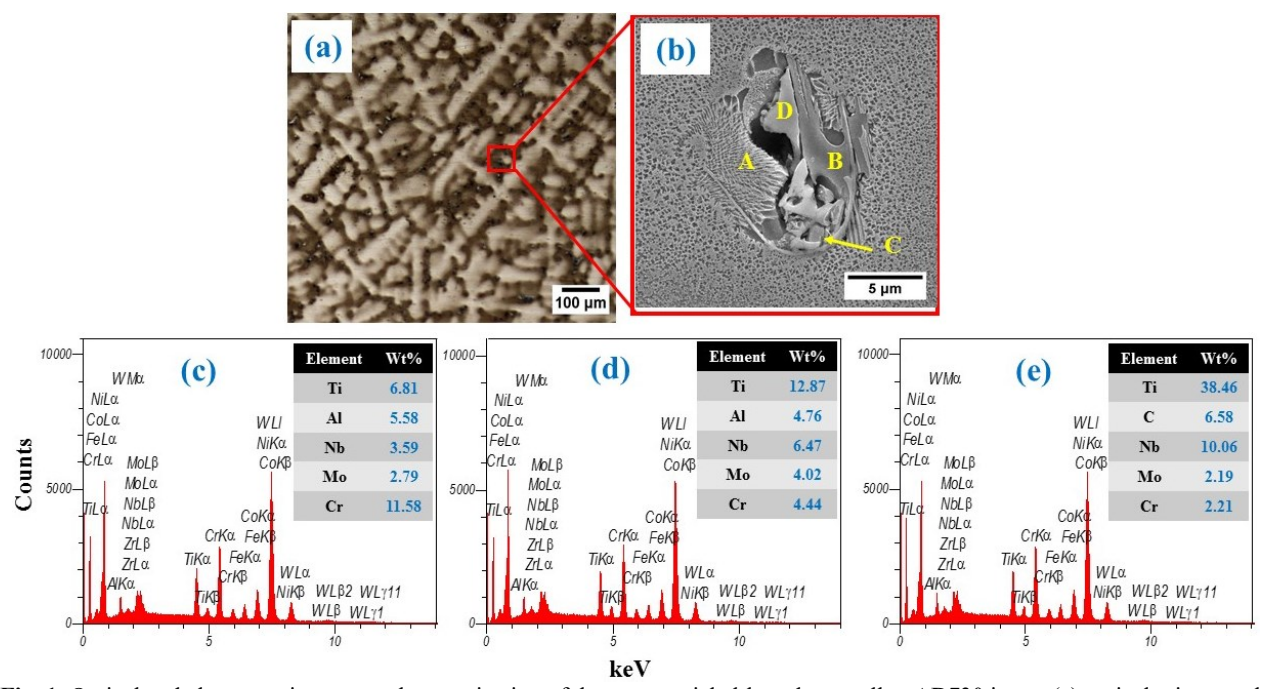


Fig. 1. Optical and electron microscopy characterization of the as-cast nickel-based superalloy AD730 ingot: (a) optical micrograph, (b) SEM image, (c) EDS spectrum of region A, (d) EDS spectrum of region B, and (e) EDS spectrum of region C.

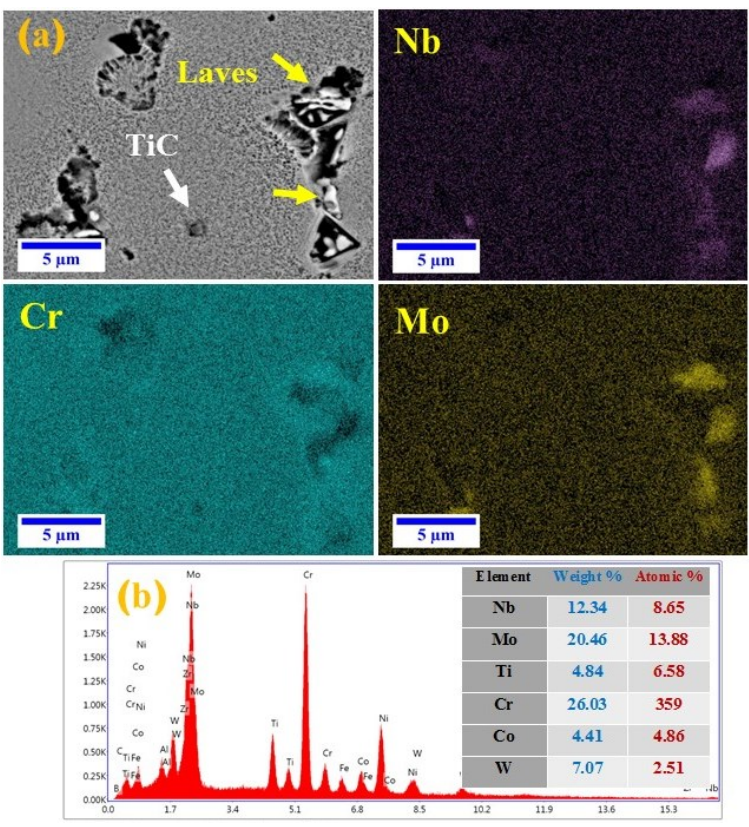


Fig. 2. (a) SEM micrograph of the phases formed in the microstructure of the AD730 superalloy, accompanied by elemental distribution maps of Nb, Mo, and Cr and (b) EDS spectrum of the Laves phase.

Table 2, presents the chemical composition of the Laves phase in various nickel-based superalloys, including the comparative results for AD730. The comparison reveals noticeable variability of the Laves phase composition in AD730 with other superalloys. For example, in Alloy 625 [21], Mo and Nb occur in significant quantities, but their ratio relative to Ni and Cr is lower than that in AD730. In contrast, in the 9K151 alloy [16], Co and contribute more dominantly to Laves phase formation, whereas the Mo content relative to Ni and Cr is reduced. Furthermore, the presence of Fe as a primary group B element in the HES-A1 alloy [22] highlights compositional differences between these systems and AD730.

These findings suggest that the Laves phase develops uniquely in each alloy and is influenced by factors

including chemical composition, solidification conditions, and heat treatment. Moreover, even minor differences in elemental percentages within this phase may substantially affect the mechanical properties of the alloy, warranting further study in future research.

3.2. STA analyses

A simultaneous thermal analysis (STA) test consisting of a heating–cooling cycle was conducted, and the results are presented in Fig. 3. During the heating stage, a distinct endothermic peak appears at approximately 1095 °C, as highlighted in the magnified view in Fig. 3(b). This peak is associated with the dissolution of γ' strengthening precipitates into the γ matrix, signifying the onset of complete dissolution at this temperature.

Table 2. Chemical composition of the Laves phase in different nickel-based superalloys (at. %)

Alloy (at%)	Ni	Fe	Co	Cr	Mo	W	Al	Ti	Nb	Ref.
AD730	21.79	3.23	4.86	32.59	13.88	2.51	5.91	6.58	8.65	This Work
ЭК151	33.40	-	19.67	20.94	8.20	0.68	3.07	3.21	9.92	[16]
Alloy 625	30.11	2.06	-	18.20	27.77	-	0.30	0.30	21.25	[21]
HES-A1 alloy	33.68	14.88	5.12	17.80	7.86	-	4.72	1.43	14.51	[22]

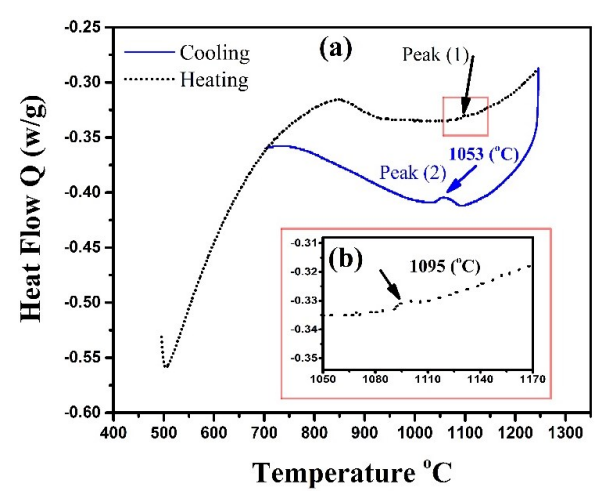


Fig. 3. STA heating and cooling curves of as-cast AD730 nickel base super alloy.

Conversely, the cooling curve exhibits a noticeable exothermic peak at around 1053 °C, corresponding to the nucleation and re-precipitation of γ' during cooling. Therefore, the complete dissolution and re-precipitation temperature of the γ' phase in this alloy occur at about 1095 °C and 1053 °C, respectively.

These findings are in good agreement with previous studies. Masoumi et al. [6] determined γ' dissolution and precipitation temperatures of 1099 °C and 1044 °C, respectively, using DTA analysis. Similarly, Mirzaei et al. [23] reported a γ' dissolution temperature of approximately 1079 °C. The slight discrepancies among different studies can be attributed to variations in chemical composition, casting parameters, initial γ' size/distribution, and the applied thermal conditions during testing.

3.3. Effect of homogenization time on microstructure

Figs. 4(a-e) illustrates the microstructural evolution of homogenized samples at a constant temperature of 1100 °C for various durations. In these micrographs, the bright regions correspond to dendrites, whereas the darker regions represent interdendritic areas. This microstructural heterogeneity arises from the segregation of alloying elements during nonequilibrium solidification. A careful examination reveals that prolonging the homogenization time leads to the progressive dissolution of dendritic structures and their transformation into a more uniform microstructure.

After 5 hours of homogenization, dendritic and interdendritic regions remain clearly distinguishable (Fig. 4(a)). When the homogenization time is extended to 10 hours, a remarkable reduction in these regions is observed (Fig. 4(b)). At this stage, the interdendritic zones are predominantly occupied by coarse γ' precipitates. This phenomenon is mainly attributed to the segregation of Al and Ti during nonequilibrium solidification, which promotes γ' precipitation and growth within the interdendritic regions [14, 24]. With further extension of the homogenization time (Figs. 4(ce))., sufficient diffusion of alloying elements is achieved, leading to fragmentation and near elimination of the dendritic structures from the microstructure. These results demonstrate the microstructural evolution driven by the homogenization process, which gradually results in a more homogeneous distribution of alloying elements throughout the sample. In other words, increasing the homogenization time provides the required conditions for effective elemental diffusion, thereby exerting a significant influence on homogenization efficiency and microstructural development [25].

Accordingly, based on the optical micrographs presented in Fig. (4), homogenization of the AD730 alloy at $1100~^{\circ}$ C, which is close to the dissolution temperature of γ' precipitates [6], indicates that dendritic structures are still retained at short homogenization durations. This morphology, originating from nonequilibrium solidification in cast ingots, is manifested as regions with non-uniform chemical composition. The persistence of such dendritic structures has also been reported in the Nibased superalloy GH4151, even after homogenization at $1200~^{\circ}$ C for 5 hours [3].

Fig. 5 presents scanning electron microscopy (SEM) images of the microstructure of samples homogenized at 1100 °C for 5, 10, 15, 20, and 25 hours. As observed in these images, at 5 hours (Fig. 5(a)), the interdendritic regions contain coarse γ' precipitates and η phase with a blade-like morphology. The volume fraction of the coarse γ' precipitates formed in the interdendritic regions under these conditions is considerable. These precipitates and phases, mainly concentrated in the interdendritic areas, clearly indicate non-equilibrium solidification and

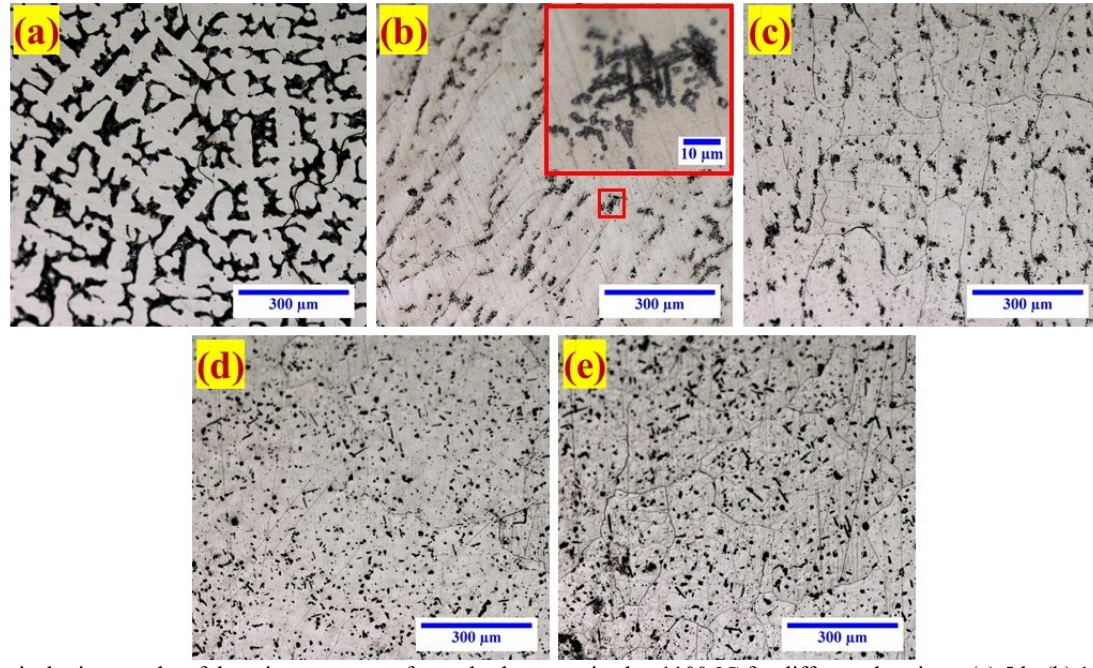


Fig. 4. Optical micrographs of the microstructure of samples homogenized at 1100 °C for different durations: (a) 5 h, (b) 10 h, (c) 15 h, (d) 20 h, and (e) 25 h.

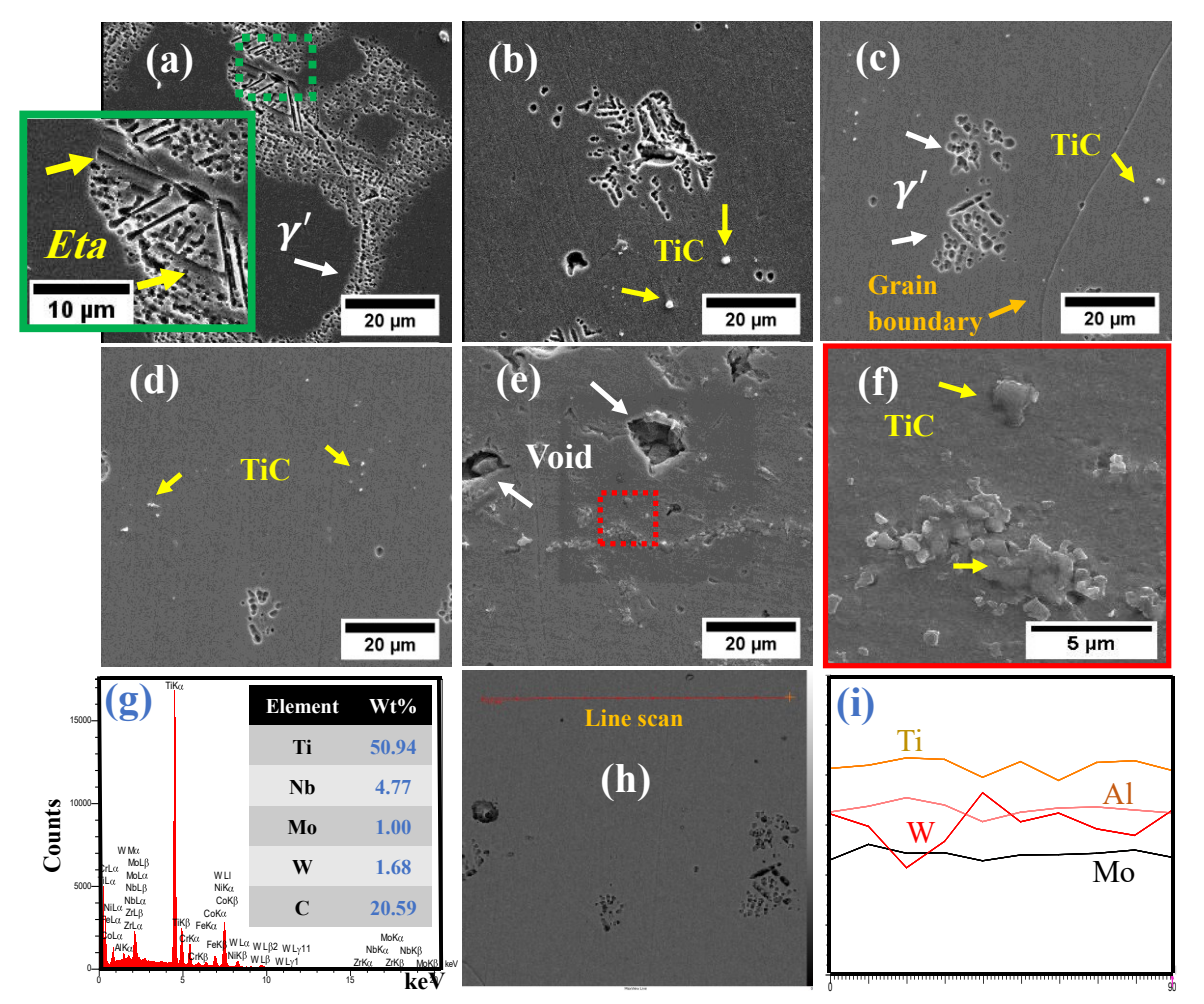


Fig. 5. SEM micrographs of the microstructure of samples homogenized at 1100 °C for (a) 5 h, (b) 10 h, (c) 15 h, (d) 20 h, and (e) 25 h; (f) high-magnification image of titanium carbides observed in (e), (g) EDS analysis confirming the composition of titanium carbides, (h) Microstructure corresponding to the sample homogenized for 15 h, and (i) line-scan elemental profiles of Ti, Al, W, and Mo across the microstructural features shown in (h).

an uneven distribution of alloying elements in the cast microstructure. A comparison of the images in Fig. 5 with those in Fig. 1(b) shows that even the shortest homogenization treatment (1100 °C for 5 hours) results in the complete dissolution of phases such as the eutectic $(\gamma + \gamma')$ from the microstructure.

Furthermore, with increasing homogenization time to 10 hours (Fig. 5(b)), the conditions necessary for atomic diffusion and distribution are further satisfied, resulting in the dissolution and elimination of the η phase from the microstructure. Therefore, increasing homogenization time from 5 to 10 hours leads to a more homogeneous microstructure, indicating an improvement in microstructural uniformity. Microscopic examinations also show that γ' precipitates, which appear as coarse particles concentrated in the interdendritic regions, are still visible in the microstructure. However, the volume fraction of these precipitates decreases markedly. This reduction reflects the gradual dissolution of γ' precipitates and phase transformations occurring during the homogenization process.

With increasing homogenization time to 15 and 20 hours (Figs. 5(c) and (d)), a significant reduction in the volume fraction of coarse γ' precipitates is observed. This evolution indicates that the dissolution process has advanced to later stages, accompanied by a decrease in microstructural inhomogeneities within the interdendritic regions. At this stage, atomic diffusion occurs more effectively, leading to a more uniform distribution of phases within the microstructure. This phenomenon reflects the microstructure's approach toward thermodynamic equilibrium the applied homogenization temperature and duration.

After 25 hours of homogenization (Fig. 5(e)), the coarse γ' precipitates are completely dissolved, and no remnants of these particles are visible in the microstructure. This complete dissolution is attributed to the extensive redistribution of key alloying elements, such as Al and Ti, into the matrix, which improves the chemical uniformity and overall microstructural homogeneity. Concurrently, a significant increase in both the volume fraction and size of MC-type TiC carbides was detected. In certain regions, these carbides exhibit an

island-like clustered morphology (Fig. 5(f)).

To further examine the chemical distribution and carbide evolution during homogenization, complementary EDS and line-scan analyses were conducted. As shown in Fig. 5(g), the energy-dispersive X-ray spectroscopy (EDS) analysis confirms the presence and chemical composition of titanium carbides in the microstructure. Fig. 5(h) illustrates the detailed microstructure of the sample homogenized for 15 h, while Fig. 5(i) presents the line-scan profiles of Ti, Al, W, and Mo across different regions of this microstructure. The results indicate that the distribution of Ti, Al, and Mo becomes nearly uniform after homogenization, with a significant reduction in compositional differences between dendritic and interdendritic regions. Tungsten exhibits a similar trend; however, a slight concentration variation is still observed, likely due to its relatively lower diffusion rate compared with the other alloying elements.

Roy [26] reported that at elevated temperatures, smaller particles may dissolve and coalesce with adjacent coarse particles or alternatively, merge with nearby fine ones. Consistent with this observation, the TiC carbides in the AD730 alloy likely underwent localized agglomeration and slight coarsening, resulting in their clustered and island-like appearance. These findings suggest that during extended homogenization, stable carbides tend to undergo localized growth and aggregation, whereas γ' precipitates gradually dissolve, thereby enhancing the chemical homogeneity of the γ matrix. Nevertheless, despite the complete dissolution of coarse γ' precipitates after 25 hours of homogenization, notable cavities were detected within the matrix.

These cavities are likely associated with extensive precipitate dissolution and pronounced redistribution of alloying elements on a microscopic scale. Such behavior can induce localized instabilities such as Kirkendall voids or vacancy clustering, contributing to the observed microstructural defects. The formation of these cavities during prolonged homogenization can be primarily attributed to the Kirkendall effect, where unequal diffusion rates of alloying species create a net flux of vacancies toward the slower-diffusing side. When the

influx of vacancies exceeds the absorption capacity of sinks such as dislocations and grain boundaries, supersaturation occurs, leading to local nucleation of voids. First-principles and molecular dynamics simulations in nickel-based systems have shown that vacancy clusters are stable and play a critical role in void formation, confirming the significance of vacancy supersaturation in these alloys [27].

In nickel-based superalloys, rapid dissolution of strengthening precipitates (e.g., γ' or carbides) during homogenization causes a marked local redistribution of alloying elements, perturbing lattice equilibrium and further enhancing vacancy supersaturation. phenomenon can trigger cavity formation even in regions distant from classical marker planes. Some studies on nickel-base superalloy [28,29] and Ni-Cr series wires [30, 31] have reported the occurrence of Kirkendall void formation at elevated temperatures homogenization, highlighting the relevance of these mechanisms to the cavities observed in AD730 after 25 hours of homogenization.

Microstructural analysis results indicate that homogenization at 1100 °C significantly reduces the amount of secondary phases, particularly coarse γ' precipitates and the η phase, leading to a more uniform distribution of alloying elements. Moreover, the increase in the size of MC carbides with longer heat treatment times indicates the stability of this phase within the AD730 alloy structure at this temperature.

Fig. 6 presents the hardness variations of the AD730 superalloy after homogenization at a constant temperature of 1100 °C for different durations. As shown, the hardness of the samples decreases uniformly with increasing homogenization time; specifically, the hardness is about 331 HB after 5 hours to 268 HB after 25 hours. This gradual decrease is mainly attributed to the dissolution of gamma prime precipitates in the microstructure. Since the homogenization temperature is close to the γ' precipitate dissolution temperature, extended exposure reduces the volume fraction of these precipitates. As the volume fraction of gamma prime decreases, its strengthening effect on the alloy diminishes, resulting in lower hardness values.

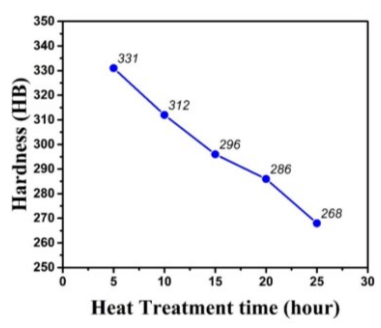


Fig. 6. Hardness variation of the AD730 superalloy as a function of homogenization time.

In addition to precipitate dissolution, prolonged homogenization promotes grain growth. Larger grains reduce the grain boundary area per unit volume, thereby decreasing the role of grain boundaries as obstacles to dislocation motion, which further contributes to hardness reduction. Therefore, the observed decrease in hardness during homogenization can be attributed to a combined effect of two time-dependent phenomena: γ' precipitate dissolution and grain coarsening.

Overall, homogenization at 1100 °C significantly influences the microstructural characteristics mechanical behavior of the AD730 superalloy. Progressive dissolution of interdendritic phases such as eutectic $(\gamma + \gamma')$, η phase, and Laves phase occurred as the homogenization time increased, promoting a more chemically uniform and structurally refined matrix. However, prolonged exposure beyond 20 hours led to undesirable effects such as void formation and excessive carbide growth. Moreover, the continuous reduction in hardness with time reflected the dissolution of strengthening γ' precipitates and grain coarsening. These findings highlight the critical balance between sufficient homogenization to eliminate segregated phases and the need to avoid over-homogenization that could degrade mechanical integrity.

4. Conclusions

In the present study, the effect of homogenization time at a constant temperature of 1100 °C on the microstructure and hardness of the AD730 superalloy was systematically investigated. The main findings are as follows:

1. Homogenization at 1100 °C resulted in the complete dissolution of eutectic $\gamma + \gamma'$ and Laves phases in the

early stages of the process, indicating a rapid and effective response in modifying the initial microstructure.

- 2. After 10 hours of homogenization, the η phase was no longer detected in the microstructure, demonstrating its full dissolution under the applied thermal conditions.
- 3. At 1100 °C and after 25 hours of treatment, the formation of voids in the microstructure became apparent. Considering that this temperature is close to the solvus temperature of γ' precipitates, such observations indicate the onset of structural instability within the alloy. Therefore, it can be concluded that the optimal homogenization time at this temperature ranges between 15 and 20 hours to prevent the development of defects.
- 4. The hardness of the alloy continuously decreased during the homogenization process, primarily due to the gradual dissolution of γ' precipitates. After 25 hours, these precipitates were completely eliminated from the microstructure, leading to a significant reduction in hardness.

Acknowledgments

The authors would like to express their sincere gratitude to Mr. Safavi for his support in metallographic sample preparation, and to Mr. Akhoundzadeh for his assistance with the heat treatment procedures during this research.

Authors' contributions

S. Mortezaei: Writing original draft, Data collection, Date analysis

S. M. Abbasi: Supervision, Writing - review & editing
M. Morakabati: Formal analysis, Writing - review & editing

Conflict of interest

The authors declare that they have no financial or personal relationships that could have inappropriately influenced or biased the work presented in this manuscript.

Funding

This research received no external funding.

5. References

- [1] Jia, L., Cui, H., Yang, S., Lv, S., Xie, X., & Qu, J. (2023). As-cast microstructure and homogenization kinetics of a typical hard-to-deform Ni-base superalloy. *Journal of Materials Research and Technology, 23*, 5368–5381. https://doi.org/10.1016/j.jmrt.2023.01.150
- [2] Li, X. X., Jia, C. L., Zhang, Y., Lü, S. M., & Jiang, Z. H. (2020). Incipient melting phase and its dissolution kinetics for a new superalloy. *Transactions of Nonferrous Metals Society of China*, 30, 2107–2118. https://doi.org/10.1016/S1003-6326(20)65364-X
- [3] Li, X. X., Jia, C. L., & Yu, A. (2023, June). Influence of homogenization degree on microstructure and mechanical properties for a novel wrought superalloy. In *Journal of Physics: Conference Series* (Vol. 2519, No. 1, p. 012040). IOP Publishing. https://doi.org/10.1088/1742-6596/2519/1/012040
- [4] Devaux, A., Picqué, B., Gervais, M. F., Georges, E., Poulain, T., & Héritier, P. (2012). AD730TM-A new nickel-based superalloy for high temperature engine rotative parts. TMS Superalloys, 911919. https://doi.org/10.7449/2012/Superalloys 2012 911 919
- [5] Devaux, A., Helstroffer, A., Cormier, J., Villechaise, P., Douin, J., Hantcherli, M., & Pettinari-Sturmel, F. (2014, November). Effect of aging heat-treatment on mechanical properties of AD730TM superalloy. In 8th International Symposium on Superalloy 718 and Derivatives (pp. 521-535). Hoboken, NJ, USA: John Wiley & Sons, Inc.

https://doi.org/10.1002/9781119016854.ch41

- [6] Masoumi, F., Jahazi, M., Cormier, J., & Shahriari, D. (2014). Dissolution kinetics and morphological changes of γ' in AD730TM superalloy. In MATEC Web of Conferences (Vol. 14, p. 13005). EDP Sciences. https://doi.org/10.1051/matecconf/20141413005
- [7] Belan, J. (2016). GCP and TCP Phases Presented in Nickel-base Superalloys. *Materials Today: Proceedings*, 3(4), 936–941.

https://doi.org/10.1016/j.matpr.2016.03.024

- [8] Li, X., Jia, C., Jiang, Z., Zhang, Y., & Lv, S. (2020). Investigation of solidification behavior in a new high alloy Ni-based superalloy. *JOM*, 72(11), 4139-4147. https://doi.org/10.1007/s11837-020-04346-7
- [9] Li, Y., et al. (2022). Study on microsegregation and homogenization process of a novel nickel-based wrought superalloy. *Journal of Materials Research and Technology*, 19, 3366–3379. https://doi.org/10.1016/j.jmrt.2022.06.088
- [10] Shui, L., & Fu, J. (2022). An investigation on as-cast microstructure and homogenization of nickel base superalloy René 65. *High Temperature. Materials and Processes.*, 41, 555–567. https://doi.org/10.1515/htmp-2022-0245

- [11] Miao, Z. J., Shan, A. D., Lu, J., & Song, H. W. (2011). Segregation and diffusion characterisation in two-stage homogenisation of conventional superalloy. *Materials Science and Technology.*, 27(10), 1551–1557. https://doi.org/10.1179/026708310X12815992418139
- [12] Blaizot, J., Finet, L., Chabrier, A., Fornara, A., Fage, M., Remichi, R., Dadé, M., & Perez, M. (2024, August). Gamma Prime Precipitation in Cast and Wrought AD730® Superalloy. In *International Symposium on Superalloys* (pp. 762-773). Cham: Springer Nature Switzerland. https://doi.org/10.1007/978-3-031-63937-1_72
- [13] Li, X. X., Jia, C. L., Zhang, Y., Lv, S. M., & Jiang, Z. H. (2020). Segregation and homogenization for a new nickel-based superalloy. *Vacuum*, 177, 109379. https://doi.org/10.1016/j.vacuum.2020.109379
- [14] Zhou, Z., Zhang, R., Cui, C., Zhou, Y., & Sun, X. (2021). Effects of homogenization treatment on the microsegregation of a Ni–Co based superalloy produced by directional solidification. *Acta Metallurgica Sinica* (English Letters) 34(7), 943–954. https://doi.org/10.1007/s40195-021-01192-7
- [15] Ruan, J. J., Ueshima, N., & Oikawa, K. (2018). Phase transformations and grain growth behaviors in superalloy 718. *Journal of Alloys and Compounds.*, 737, 83–91. https://doi.org/10.1016/j.jallcom.2017.11.327
- [16] Tan, Y. G., et al. (2019). Element segregation and solidification behavior of a Nb, Ti, Al co-strengthened superalloy 3K151. Acta Metallurgica Sinica (English Letters), 32, 1298–1308. https://doi.org/10.1007/s40195-019-00894-3
- [17] Ling, L., Han, Y., Zhou, W., Gao, H., Shu, D., Wang, J., Kang, M., & Sun, B. (2015). Study of microsegregation and Laves phase in INCONEL718 superalloy regarding cooling rate during solidification. *Metallurgical and Materials Transactions A*, 46, 354–361. https://doi.org/10.1007/s11661-014-2614-5
- [18] Wilson, A. S. (2016). Formation and effect of topologically close-packed phases in nickel-base superalloys. *Materials Science and Technology*, 33(9), 1108-1118.
 - https://doi.org/10.1080/02670836.2016.1187335
- [19] Stein, F. (2020). Laves phases: a review of their functional and structural applications and an improved fundamental understanding of stability and properties *Journal of Materials Science*, 56(9), 5321-5427. https://doi.org/10.1007/s10853-020-05509-2
- [20] Floreen, S., Fuchs, G. E., & Yang, W. J. (1994). The metallurgy of alloy 625. *Superalloys*, 718(625), 13-37. https://doi.org/10.7449/1994/superalloys 1994 13 37
- [21] Chen, W. (2000). Composition effects on macroscopic solidification segregation of superalloys. West Virginia University. https://doi.org/10.33915/etd.1229

[22] Shafiee, A., Nili-Ahmadabadi, M., Kim, H. S., & Jahazi, M. (2020). Development and microstructural characterization of a new wrought high entropy superalloy. *Metals and Materials International*, 26(5), 591–602. https://doi.org/10.1007/s12540-019-00360-w

- [23] Mirzaie, Z., Ebrahimi, G. R., Ezatpour, H., & Ali Akbari Sani, S. (2021). Hot deformation behavior and development of constitutive equations on a novel γ-γ/Nibase superalloy AD730. *Iranian Journal of Materials Forming*, 8(3), 4-17.
 - https://doi.org/10.22099/IJMF.2021.40096.1179
- [24] Zhuang, X., Tan, Y., Zhao, L., You, X., Li, P., & Cui, C. (2020). Microsegregation of a new Ni-Co-based superalloy prepared through electron beam smelting and its homogenization treatment, *Journal of Materials Research and Technology*, 9(3), 5422-5430. https://doi.org/10.1016/j.jmrt.2020.03.068
- [25] Chen, K., Rui, S., Wang, F., Dong, J., & Yao, Z. (2019). Microstructure and homogenization process of as-cast GH4169D alloy for novel turbine disk, *International Journal of Minerals*, *Metallurgy, and Materials*, 26(7) 889–900. https://doi.org/10.1007/s12613-019-1802-0
- [26] Roy, I., Balikci, E., Ibekwe, S., & Raman, A. (2005). Precipitate growth activation energy requirements in the duplex size γ' distribution in the superalloy IN738LC, *Journal of Materials Science*, 40(23), 6207-6215. https://doi.org/10.1007/s10853-005-3154-6
- [27]Zhao, S., Zhang, Y., & Weber, W. J. (2018). Stability of vacancy-type defect clusters in Ni based on firstprinciples and molecular dynamics simulations. *Scripta Materialia*, 145, 71-75.
 - https://doi.org/10.1016/j.scriptamat.2017.10.003
- [28] Anton, D. L., & Giamei, A. F. (1985). Porosity distribution and growth during homogenization in single crystals of a nickel-base superalloy. *Materials Science and Engineering*, 76, 173-180.
 - https://doi.org/10.1016/0025-5416(85)90091-6
- [29] Epishin, A., Link, T., Svetlov, I. L., Nolze, G., Neumann, R. S., & Lucas, H. (2013). Mechanism of porosity growth during homogenisation in single crystal nickel-based superalloys. *International Journal of Materials Research*, 104(8), 776-782.
 - https://doi.org/10.3139/146.110924
- [30]y Puente, A. P., & Dunand, D. C. (2018). Effect of Cr content on interdiffusion and Kirkendall pore formation during homogenization of pack-aluminized Ni and Ni-Cr wires. *Intermetallics*, 101, 108-115.
 - https://doi.org/10.1016/j.intermet.2018.07.007
- [31] y Puente, A. P., Erdeniz, D., Fife, J. L., & Dunand, D. C. (2016). In situ X-ray tomographic microscopy of Kirkendall pore formation and evolution during homogenization of pack-aluminized Ni–Cr wires. *Acta Materialia*, 103, 534-546. https://doi.org/10.1016/j.actamat.2015.10.013